

**Implementation of the Sanchez-Pomraning Double Heterogeneity
Treatment Method in DeCART**

September 2007

Leonid Pogosebkyan and Han Gyu Joo

Reactor Physics Laboratory
Seoul National University

Abstract

The Sanchez-Pomraning method to resolve the double heterogeneity (DH) in the method of characteristics (MOC) transport calculation, which we call DH MOC, is implemented into the DeCART code for the application of the DeCART code to the gas cooled reactors involving particulate triso fuels. Since the DH MOC requires essentially no modification of the existing MOC calculation module other than providing the effective macroscopic cross section and the effective source constructed from the stochastic material properties and micro regional source, implementation is focused on the variable structure changes to incorporate micromaterials and the pre and post processing for the DH MOC calculation. The DH MOC solver is incorporated first in the shielded resonance cross section determination and then as in the normal MOC transport solution. As a prerequisite for the implementation of the DH MOC solver, a method to determine the volume to volume collision probabilities (CP) for a sphere is derived in detail. The verification of the CP routines and other code modifications are performed using various analytical solutions. The final verification of the DH MOC is performed by comparing the DeCART DH MOC results with the MCNP results obtained with an explicit representation of the particulate fuels. The effect of double heterogeneity on the resonance cross section and on the normal MOC transport calculation are assessed separately.

Table of Contents

Abstract	
1. Introduction	1
2. General Elements and Procedure Required for DH MOC	3
2.1 Symbols and Formulae	4
2.2 Calculation Sequence	7
2.3 Evaluation of Collision Probabilities for Spherical Triso-Particles	11
2.4 Verification of Collision Probability Routine Using Analytic Solutions	14
2.4.1 Transmission Probability	14
2.4.2 Volume-to-Surface Escape Probability	16
3. Specifics of DH MOC Implementation into DeCART	18
3.1 Change of Variable Structure	18
3.2 Program Logic Changes	20
3.2.1 Two Loops to Treat Micromaterials	20
3.2.2 Non-Iterating Part of Ray Tracing Preprocessor	22
3.2.3 Modification of Ray Tracing Driver Routines	23
3.3 Input Description and Sample Inputs	24
4. Verifications of the Implementation	26
4.1 DH MOC Subgroup Solution for a Single Cell	26
4.2 Micro Heterogeneity Only	27
4.3 Macro-heterogeneity Only at the Pin Cell Level	29
4.4 Assessment of DH effect in Practical Problems	30
5. Conclusions	34
References	35

1. Introduction

This report is to describe the practical aspects of the implementation in DeCART code¹ of the Sanchez-Pomraning method^{2,3} which is given with exhaustive details in the companion report⁴. This work was initiated by the need for the application of the DeCART whole transport code to the block-type Very High Temperature Reactors (VHTRs). These reactors employ prismatic hexagonal fuel blocks in which cylindrical fuel compacts containing coated fuel particles are loaded. The coated fuel particles having a diameter of ~0.5 mm, called TRISO particles (TRIStructural ISOTropic), are randomly distributed in the graphite matrix. The multiple coating provides a miniature containment vessel for the fuel seed to retain inside gaseous fission products even under the very high operating temperature conditions. These triso fuels bring in two levels of heterogeneity. The first level (macro-level) is formed by the heterogeneous arrangement of the fuel and other components in the reactor, while the second level (micro-level) is formed by the TRISO particles in the compact.

The most difficult problem appearing in the VHTR neutronic analysis is the resolution of the effect of double heterogeneity (DH) on the resonance self-shielding of cross sections and on the neutron transport. The DH effect on the resonance self-shielding can be mitigated by proper modifications of the DeCART resonance treatment module that is based on solving the resonance fixed source transport equation¹ to determine the subgroupwise fluxes with the method of characteristic (MOC) solver. Particularly, the DeCART code should be extended to solve the same fixed source transport equations in a doubly heterogeneous stochastic medium. The non-resonance part of DH effect is supposed to be much smaller, but not negligible. The method to treat the DH in the MOC calculation was initially derived by Sanchez² and also explained with a sufficient detail in Reference⁴. We designate this method as DH MOC. Although, the DH MOC is known, there are a lot of things to be resolved for the actual implementation and this report describes the specific details of the implementation.

In the following section, the general element and procedures needed for the implementation of DH MOC in DeCART are described. This section provides a complete set of symbols and formulae and the calculation algorithm. It also gives a detailed derivation of the collision probability for a heterogeneous sphere. Various analytic verifications of the collision probability routines are also provided. The details of the implementation of DH MOC in DeCART are described in Section 2, which requires a large amount of changes in the coding

including the variable names changes in order to incorporate micromaterials and subregions and the logic changes to implement the logic changes. The description of the new input cards to describe the composite material is also given in Section 3. The verification of the implementation is done in various ways in Section 4. It is culminated at the assessment of the DH effect for a set of practical problems. The DeCART DH results are compared with the MCNP results and an assessment of the DH effect in the resonance cross section only is made as well.

2. General Elements and Procedure Required for DH MOC

The need for an explicit double heterogeneity (DH) treatment can be judged by an optical size criterion. If the following inequality is valid,

$$\left| \Sigma_{matrix} - \Sigma_{grain} \right| \cdot d_{grain} > \varepsilon \quad (1)$$

where d_{grain} is the grain diameter and ε is the limiting optical length of about 0.1 which gives about 10% reduction in the flux, the volume-weighted homogenization of micro grains is unacceptable due to the large flux variation within micro grains. For a typical grain kernel size of about 0.04 cm, the above condition gives 2.5 cm⁻¹ for the macroscopic cross section. With the typical value of the Uranium number density of 0.025 atoms/cm³ and the enrichment of 10% in the VHTR fuels, this macroscopic cross section corresponds to ~110 barns for U-238 and ~1000 barns for U-235. Since near the resonances of U-238, the 110 barn condition can be met easily, all the resonance calculation should be done considering the enhanced self-shielding due to the double heterogeneity. On the contrary, it is expected that the other energy groups than the resonance groups, only a few thermal groups which would have a large microscopic cross section require the treatment of the DH. In this regard, the DH implementation will be concentrated on the resonance shielding calculation which involves the solution of the following subgroup fixed source problem in DeCART:

$$\boldsymbol{\Omega} \cdot \nabla \psi(\mathbf{r}, \boldsymbol{\Omega}) + (\Sigma_{am}(\mathbf{r}) + \Sigma_s(\mathbf{r}))\psi(\mathbf{r}, \boldsymbol{\Omega}) = \frac{1}{4\pi} \lambda \Sigma_p(\mathbf{r}) + \frac{1}{4\pi} (1 - \lambda) \Sigma_s(\mathbf{r}) \Phi(\mathbf{r}) \quad (2)$$

where

$\psi(\mathbf{r}, \boldsymbol{\Omega})$ = angular flux,

$\Phi(\mathbf{r})$ = scalar flux,

$\Sigma_{am}(\mathbf{r})$ = absorption cross section for subgroup level m,

$\Sigma_s(\mathbf{r})$ = scattering cross section,

$\lambda \Sigma_p(\mathbf{r})$ = potential scattering cross section multiplied by the intermediate resonance parameter.

In the following, the complete set of formulae needed for the DH MOC solution of the above equation is given starting from the definition of all the symbols. Since the DH MOC method by Sanchez-Pomraning requires the escape probabilities which can be determined from the volume-to-volume collision probabilities, a method for determining the collision probability

for a sphere derived in Section 2.2. The verification of the collision probability routine by analytic solution is given in Section 2.3. The entire calculation sequence is described at last. Nomenclature of basic variables and basic formula

2.1 Symbols and Formulae

The following notations will be used in the formulae to follow. All the symbols and formulae can be found in Reference 4.

0	= (carbon) matrix index,
i	= type-of-grain index $i = 1, \dots, M$,
k	= index of grain's layer,
g	= grain label,
m	= index of subgroup level,
p_0	= volumetric fraction for matrix,
p_i	= volumetric fraction for grains ($i > 0$),
V_{ik}^g	= volume of layer k of grain i ,
r_{ik}^g	= external radius of layer k of grain i ,
p_{ik}^g	= volumetric fraction of layer k within grain i ,
p_{ik}	= volumetric fraction of layer ki with respect to the entire material,
$\Sigma_{am, ik}$	= absorption cross section for grain i and layer k for subgroup level m ,
Σ_{ik}	= total cross section for grain i and layer k ,
$\Sigma_{s, ik}$	= scattering cross section for grain i and layer k ,
$\Sigma_{am, 0}$	= absorption cross section for matrix, corresponding to subgroup level m ,
Σ_0	= total cross section for matrix,
$\Sigma_{s, 0}$	= scattering cross section for matrix,
S_i^g	= external surface of grain i ,
$P_{ik;il}^g$	= collision probability from layer l to layer k within grain i ,
r_c	= normalizing coefficient to enforce neutron balance in DH MOC,
β	= transmission coefficient ($\beta = 1 - e^{-\Sigma L}$) along MOC trajectory L,

- β_c = normalized transmission coefficient ($\beta_c = r_c \cdot \beta$) along MOC trajectory L,
 $\lambda \Sigma_{p,0}$ = intermediate resonance parameter times potential scattering in matrix,
 $\lambda \Sigma_{p,ik}^g$ = intermediate resonance parameter times potential scattering for grain i and layer k ,
 q_0 = isotropic neutron source in matrix,
 q_{ik} = isotropic neutron source in layer k of grain i ,
 E_{ik}^g = escape probability from layer k of grain i to the surface of grain,
 \hat{E}_{ik}^g = reduced escape probability from layer k of grain i to the surface of grain,
 Σ = homogenized cross section calculated for current MOC region,
 q = effective source in heterogeneous media for MOC formula,
 Φ_{as} = (asymptotic) uncollided scalar flux for matrix, induced by internal sources only,
 Φ_{ik} = scalar flux at ik -layer resulting from internal sources q_{il} ,
 $\bar{\Phi}_{ik}$ = scalar flux of layer k of grain i (averaged by MOC region),
 $\bar{\Phi}_0$ = scalar flux in matrix (averaged by MOC region).

The following formulae will be used in the calculation sequence.

$$p_{ik}^g = V_{ik}^g / \sum_{k=1}^K V_{ik}^g \quad (3)$$

$$p_{ik} = p_i \cdot p_{ik}^g \quad (4)$$

$$\Sigma_{ik} = \Sigma_{am,ik} + \Sigma_{s,ik} \quad (5)$$

$$\Sigma_0 = \Sigma_{am,0} + \Sigma_{s,0} \quad (6)$$

(Remark: $\Sigma_{am,ik} = 0$ and $\Sigma_{am,0} = 0$ for non-resonant material)

$$\mathbf{e} = \frac{\mathbf{r}' - \mathbf{r}}{|\mathbf{r}' - \mathbf{r}|}, \quad \tau(\mathbf{r}', \mathbf{r}) = \int_0^{|\mathbf{r}' - \mathbf{r}|} \Sigma_{tot}(\mathbf{r} - l \cdot \mathbf{e}) dl \quad \text{- optical path,} \quad G(\mathbf{r}', \mathbf{r}) = \frac{e^{-\tau(\mathbf{r}', \mathbf{r})}}{4\pi |\mathbf{r}' - \mathbf{r}|^2} \quad (7)$$

$$\tilde{\Sigma} = \Sigma_0 + \frac{1}{P_0} \sum_{i=1}^M \sum_{k=1}^K p_{ik} \cdot \Sigma_{ik} \cdot E_{ik}^g \quad (8)$$

$$\begin{cases} \Sigma^{(n+1)} = \Sigma_0 + \frac{1}{P_0} \sum_{i=1}^M \sum_{k=1}^K p_{ik} \cdot (\Sigma_{ik} - \Sigma^{(n)}) \cdot \hat{E}_{ik}^g(\Sigma^{(n)}) \\ \Sigma = \lim_{n \rightarrow \infty} \Sigma^{(n)} \quad \text{- iterative formula for getting homogenized cross section } \Sigma \end{cases} \quad (9)$$

$$r_c = p_0 + \sum_{i=1}^M \sum_{k=1}^K p_{ik} \hat{E}_{ik} \quad (10)$$

$$\beta = 1 - e^{-\Sigma L} \quad (11)$$

$$\beta_c = r_c \cdot \beta \quad (12)$$

$$P_{ik;il}^g = \frac{1}{V_{ik}^g} \int_{V_{ik}^g} dV \int_{V_{il}^g} \Sigma_{ik} \cdot G(\mathbf{r}', \mathbf{r}) dV' \quad (13)$$

$$E_{ik}^g = \frac{1}{V_{ik}^g} \int_{S_i^g} dS \int_{V_{ik}^g} G(\mathbf{r}', \mathbf{r}) dV' \quad (14)$$

$$\hat{G}(\mathbf{r}', \mathbf{r}) = \frac{e^{-\tau(\mathbf{r}', \mathbf{r}) + \Sigma |\mathbf{r}' - \mathbf{r}|}}{4\pi |\mathbf{r}' - \mathbf{r}|^2} \quad (15)$$

$$\hat{E}_{ik}^g(\Sigma) = \frac{1}{V_{ik}^g} \int_{S_i^g} dS \int_{V_{ik}^g} \hat{G}(\mathbf{r}', \mathbf{r}) dV' \quad (16)$$

$$q_{ik} = \lambda \Sigma_{p, ik}^g + (\Sigma_{s, ik}^g - \lambda \Sigma_{p, ik}^g) \bar{\Phi}_{ik} \quad \text{- internal source in grain } i \text{ layer } k \quad (17)$$

$$q_0 = \lambda \Sigma_{p, 0} + (\Sigma_{s, 0} - \lambda \Sigma_{p, 0}) \bar{\Phi}_0 \quad \text{- internal source in matrix} \quad (18)$$

$$\Phi_{as} = \left(q_0 + \frac{1}{p_0} \sum_{i=1}^M \sum_{k=1}^K p_{ik} \cdot q_{ik} E_{ik} \right) / \tilde{\Sigma} \quad (19)$$

- scalar flux for matrix, induced by internal sources

$$q(\mathbf{r}) = \Sigma(\mathbf{r}) \cdot \Phi_{as}(\mathbf{r}) \quad (20)$$

The following equation is to be solved by the MOC solver of DeCART

$$\mathbf{\Omega} \cdot \nabla \psi(\mathbf{r}, \mathbf{\Omega}) + \Sigma(\mathbf{r}) \psi(\mathbf{r}, \mathbf{\Omega}) = q(\mathbf{r}) \quad (21)$$

which finds the region-averaged scalar flux for the matrix and the region outgoing current by

$$\bar{\Phi}_0 = \frac{1}{4\pi \Delta V} \int_{\Delta V} \int_{4\pi} \psi(r, \mathbf{\Omega}) d\Omega dV \quad \text{and} \quad \varphi_{out} - \varphi_{in} = \beta_c \cdot (\varphi_{as} - \varphi_{in}) \quad (22)$$

The grain flux is then determined by:

$$\Phi_{ik} = \frac{1}{V_{ik}^g \Sigma_{ik}^g} \sum_{l=1}^K V_{il}^g q_{il} P_{ik;il}^g \quad \text{- scalar flux at } ik\text{-layer resulting from internal sources } q_{il} \quad (23)$$

$$\bar{\Phi}_{ik} = \hat{E}_{ik}^g \bar{\Phi}_0 + (E_{ik}^g - \hat{E}_{ik}^g) \Phi_{as} + \Phi_{ik} \quad (24)$$

- region averaged scalar flux in the layer k of grain i .

2.2 Calculation Sequence

The calculation sequence to realize the DH MOC calculation is as follows:

- 1) Obtain the material and geometry data from the additional user input for double-heterogeneous regions.

It is assumed that the heterogeneous media consists of the matrix (graphite) and M-types of randomly distributed grains. Grains are contains k-layers. The following geometry and material data should be specified by user.

$$p_0, p_i, p_{ik}^g, \Sigma_{a, ik}, \Sigma_{ik}, \Sigma_{s, ik}, \Sigma_{a,0}, \Sigma_0, \Sigma_{s,0}$$

- 2) Perform preprocessing to determine the following value prior to the MOC iterations (listed in order of preparation).

$$p_{ik}, \tilde{\Sigma}, \Sigma, r_c, P_{ik;il}^g, V_{il}^g, E_{ik}^g, \hat{E}_{ik}^g, q_{ik}, q_0, \Phi_{as}, q$$

The above parameters can be calculated by formulae (3)-(20). Note that the homogenized cross section Σ requires iteration by Eq. (9).

- 3) Perform the MOC calculation to determine $\bar{\Phi}_0$ at all regions

- 4) Perform the post processing. ro determine $\Phi_{ik}, \bar{\Phi}_{ik}$.

2.3 Evaluation of Collision Probabilities for Spherical Triso-Particles

In the above calculation sequence, the volume-to-volume collision probabilities given by Eq. (13) is required for concentric spheres to determine the escape probabilities. This can be done by the Kavenoky technique [5,6]. Owing to the inherent symmetry of concentric spheres, the standard way of counting probabilities for isotropic emitters leading to the multiple integration can be remarkably simplified by reducing the problem to the counting probabilities for the mono directed source emitting the neutrons at hemi-space (see Figure 1). Indeed, considering single particles crossing heterogeneous sphere, we can conclude that optical path is only dependent on angle θ between particle trajectory and radius, connecting a particle location and center of sphere. Then, the 8 uniformly distributed mono-directed particles depicted at Figure 1-C pass identical optical path through the sphere as 8 isotropically emitted particles at Figure 1-D. Figure 1 only intuitively explains the reason, why isotropically uniformly emitted particles have identical first flight collision probability compared to the mono-directed uniformly emitted particles. A rigorous consideration, however, requires a strong proof that particles from uniform mono-directed source have identical angular distribution by θ (angle between trajectory and radius, connecting a particle location with center of sphere) compared to the particles from isotropic uniform source¹, and hence identical optical path distribution by θ and hence identical collision probabilities. That gives a reason for employing mono - directed source for counting collision probabilities in our specific case.

Consider s uniform mono-directed source inside spherical shell $V_i = \{\vec{x} : R_{i-1} \leq |\vec{x}| \leq R_i\}$ emitting

$$q_i = \frac{1}{V_i} = \frac{3}{4\pi(r_i^3 - r_{i-1}^3)} \quad (25)$$

particles per unit volume per unit time. Total emitting rate from volume V_i equal to 1. Then, collision probability $P_{j \leftarrow i}$ equals to collision rate in region $V_j = \{\vec{x} : R_{j-1} \leq |\vec{x}| \leq R_j\}$. Let us count it. Owing to the well known reciprocity relation,

$$V_j \sum_j P_{i \leftarrow j} = V_i \sum_i P_{j \leftarrow i} \quad (26)$$

¹ Angular distribution by θ for the both cases can be easily obtained in the spirit of derivation formula (42).

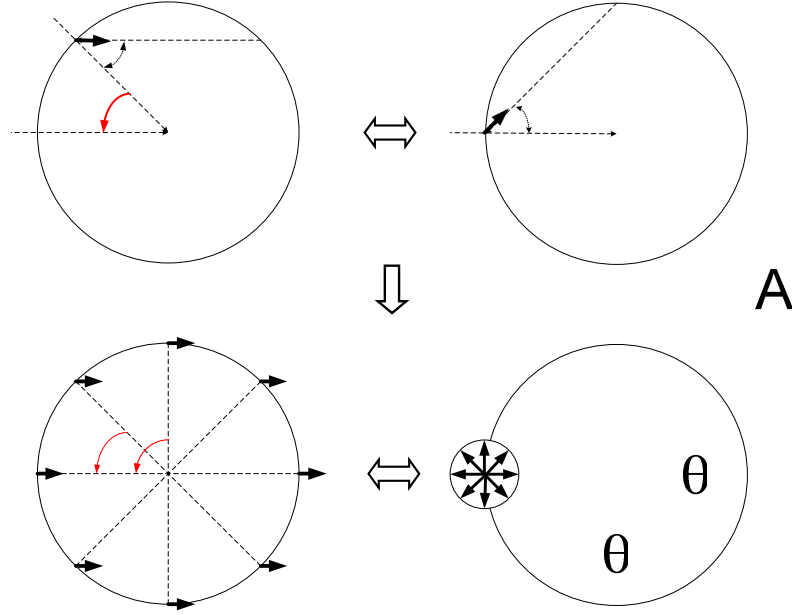


Figure 1. Use of symmetry for evaluation first-flight collision probabilities.

we can count collision probabilities for the case of $R_i \leq R_j$ then, we can obtain remaining probabilities by using formula (26). For the forward considerations we need to count optical path for the neutrons, moving along trajectories located on the distance r from spherical center as shown at Figure 2. The optical paths of interest $\tau_k(r)$, $\tau_{ij}^-(r)$, $\tau_{ij}^+(r)$ can be expressed as:

$$\tau_k(r) = \begin{cases} \Sigma_k \cdot \left(\sqrt{R_k^2 - r^2} - \sqrt{R_{k-1}^2 - r^2} \right) & \text{for } R_{k-1} \geq r \\ \Sigma_k \cdot \sqrt{R_k^2 - r^2} & \text{for } R_{k-1} < r < R_k \\ 0 & \text{for } R_k < r \end{cases} \quad (27)$$

$$\tau_{ij}^-(r) = \begin{cases} \sum_{k=i+1}^j \tau_k(r) & \text{for } i < j \\ 0 & \text{for } i \geq j \end{cases} \quad (28)$$

$$\tau_{ij}^+(r) = 2 \sum_{k=1}^i \tau_k(r) + \tau_{ij}^-(r) \quad (29)$$

where Σ_k is macro cross section and $\tau_k(r)$ is elemental optical path corresponding to volume V_k .

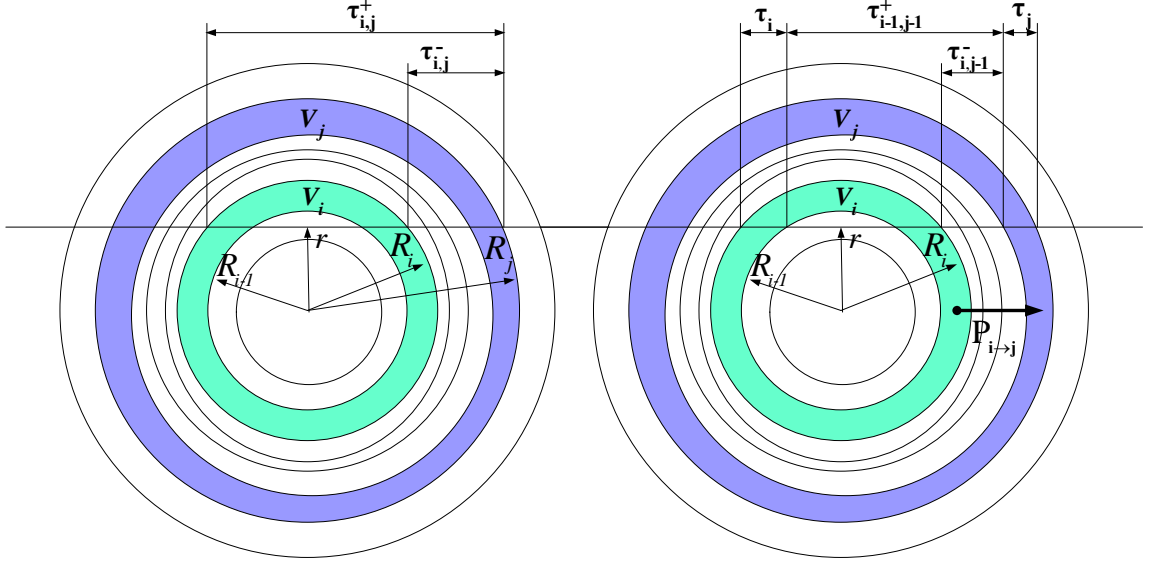


Figure 2. Notations for counting optical paths.

Consider cylinder 1 depicted at Figure 3. It has thickness dr , internal radius r and height $H(r) = \sqrt{R_i^2 - r^2} - \sqrt{R_{i-1}^2 - r^2} = \tau_i(r)/\Sigma_i$. Number of the first-flight neutrons, emitted by cylinder 1 and reached its right edge equals to:

$$q_i \int_0^H 2\pi r e^{-\Sigma_i h} dh dr = \frac{q_i}{\Sigma_i} \left(1 - e^{-\Sigma_i H}\right) 2\pi r dr = \frac{1}{\Sigma_i V_i} \left(1 - \text{Exp}(-\tau_i)\right) 2\pi r dr \quad (30)$$

The only fraction $\text{Exp}(-\tau_{i-1,j-1}^+)$ of the first-flight neutrons overcomes optical path $\tau_{i-1,j-1}^+$ from the right edge of cylinder 1 to the left edge of cylinder 2. Among of neutrons, reaching the left edge of cylinder 2 the only $\text{Exp}(-\tau_j)$ part of them could be able to reach the right edge, while remaining part $(1 - \text{Exp}(-\tau_j))$ will have collision within cylinder 2. So, number of first-flight neutrons, emitted by cylinder 1 and collided within cylinder 2 is given by:

$$\frac{1}{\Sigma_i V_i} \left(1 - \text{Exp}(-\tau_i)\right) \text{Exp}(-\tau_{i-1,j-1}^+) \left(1 - \text{Exp}(-\tau_j)\right) 2\pi r dr \quad (31)$$

Integration by r from 0 to R_i gives collision rate of first-flight neutrons emitted by the left hemisphere of V_i . In the similar way can be obtained collision rate of the first flight neutrons,

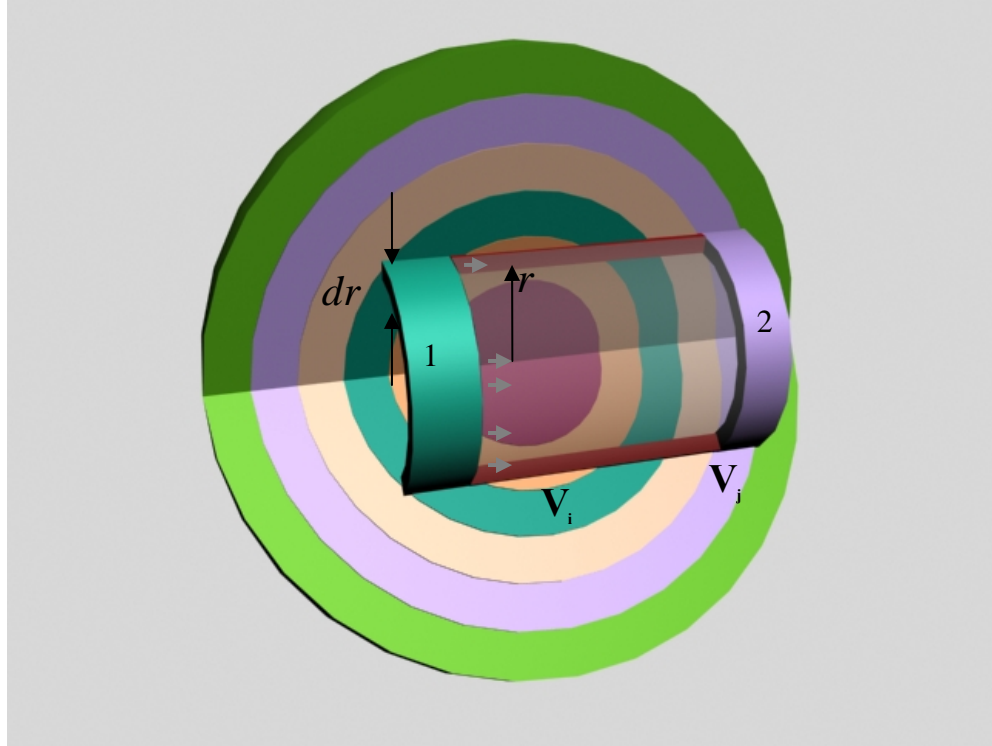


Figure 3. Evaluation of volume-to-volume collision probability

emitted by right hemisphere of V_i . In the integration over right hemisphere we have the following terms:

$$\frac{1}{\Sigma_i V_i} (1 - \text{Exp}(-\tau_i)) 2\pi r dr = \text{number of neutrons, emitted by internal cylinder;}$$

$$\text{Exp}(-\tau_{ij-1}^-) = \text{fraction of neutrons, overcoming the distance between } V_i \text{ and } V_j ;$$

$$(1 - \text{Exp}(-\tau_j)) = \text{fraction of neutrons, collided in } V_j .$$

Thus, volume-to-volume collision probability $P_{j \leftarrow i}$ equals

$$\begin{aligned} P_{j \leftarrow i} = & \int_0^{R_i} \frac{1}{\Sigma_i V_i} (1 - \text{Exp}(-\tau_i)) \text{Exp}(-\tau_{i-1, j-1}^+) (1 - \text{Exp}(-\tau_j)) 2\pi r dr + \\ & + \int_0^{R_i} \frac{1}{\Sigma_i V_i} (1 - \text{Exp}(-\tau_i)) \text{Exp}(-\tau_{i-1, j-1}^-) (1 - \text{Exp}(-\tau_j)) 2\pi r dr \end{aligned} \quad (32)$$

Using relationships

$$\begin{aligned}\tau_{i,j}^+ &= \tau_i + \tau_{i-1,j-1}^+ + \tau_j \\ \tau_{i,j-1}^+ &= \tau_i + \tau_{i-1,j-1}^+\end{aligned}\quad (33)$$

$$\begin{aligned}\tau_{i-1,j}^+ &= \tau_{i-1,j-1}^+ + \tau_j \\ \tau_{i,j-1}^- &= \tau_i + \tau_{i,j-1}^- + \tau_j \\ \tau_{i-1,j-1}^- &= \tau_i + \tau_{i,j-1}^- \\ \tau_{i,j}^- &= \tau_{i,j-1}^- + \tau_j\end{aligned}\quad (34)$$

and notation

$$\tilde{S}_{i,j}(r) = 2\pi r \left(\text{Exp}(-\tau_{i,j}^+) - \text{Exp}(-\tau_{i,j}^-) \right) \quad (35)$$

we can recast (32) in the form

$$P_{j \leftarrow i} = \frac{1}{\sum_i V_i} \int_0^{R_i} \left(\tilde{S}_{i,j} + \tilde{S}_{i-1,j-1} - \tilde{S}_{i-1,j} - \tilde{S}_{i,j-1} \right) dr \quad (36)$$

Integration (36) is performed numerically, by using Gauss integration technique. Prior doing integration, the whole range of integration $[0, R_i]$ should be subdivided into subranges

$$[0, R_i] = \bigcup_{k=1}^i [R_{k-1}, R_k] \quad (37)$$

of high degree of smoothness of integrated function, and only then Gauss integration technique can be successively implemented on the each subrange $[R_{k-1}, R_k]$. Note, evaluation of collision probability in spherical geometry requires Gauss integration technique unlike to the Gauss-Jacobi integration technique that usually is employed at cylindrical geometry. The last type of integration is relevant for singular Bikley functions, appearing in cylindrical geometry, while Gauss integration is convenient for smooth functions (35). Finally, collision probability $P_{j \leftarrow i}$ for $i < j$ is obtained by formula

$$P_{j \leftarrow i} = \frac{1}{\sum_i V_i} \sum_{k=1}^i \int_{R_{k-1}}^{R_k} \left(\tilde{S}_{i,j} + \tilde{S}_{i-1,j-1} - \tilde{S}_{i-1,j} - \tilde{S}_{i,j-1} \right) dr \quad (38)$$

where integrals $\int_{R_{k-1}}^{R_k} \left(\tilde{S}_{i,j} + \tilde{S}_{i-1,j-1} - \tilde{S}_{i-1,j} - \tilde{S}_{i,j-1} \right) dr$ are obtained numerically with Gauss integrations technique. Integrated function is given by formulae (27)-(29), (35).

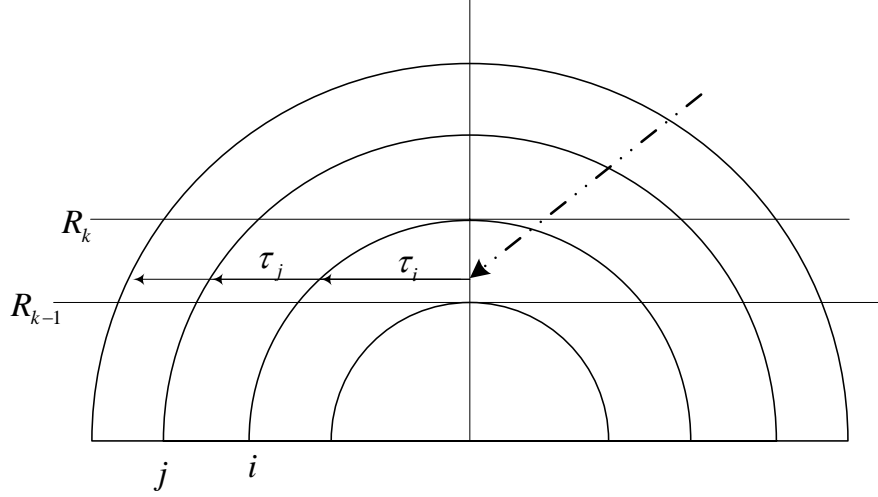


Figure 4. Implementation of Gauss integration technique.

For the case of self collision V_i to V_i the similar counting gives:

$$P_{i \leftarrow i} = \int_0^{R_i} \frac{1}{\Sigma_i V_i} (1 - \text{Exp}(-\tau_i)) \text{Exp}(-\tau_{i-1, i-1}^+) (1 - \text{Exp}(-\tau_i)) 2\pi r dr + \int_0^{R_i} \frac{2}{\Sigma_i V_i} (\tau_i + \text{Exp}(-\tau_i) - 1) 2\pi r dr \quad (39)$$

leading to the numerical integration

$$P_{i \leftarrow i} = \frac{1}{\Sigma_i V_i} \sum_{k=1}^i \int_{R_{k-1}}^{R_k} 2\pi r \left[(1 - \text{Exp}(-\tau_i))^2 \text{Exp}(-\tau_{i-1, i-1}^+) + 2(\tau_i + \text{Exp}(-\tau_i) - 1) \right] dr \quad (40)$$

Using the reciprocity (26), we obtain collision probability $P_{j \leftarrow i}$ for $i > j$. Then, using probability balance equation

$$E_i + \sum_{j=1}^N P_{j \leftarrow i} = 1 \quad (41)$$

we obtain the first flight escape probability E_i , required for MOC-DH calculations.

2.4 Verification of Collision Probability Routine Using Analytic Solutions

The collision probability routine employing the algorithm described above can be made without much effort. But it turned out that a routine is already available. This is the SYBALS routine of the DRAGON code[6]. The verification of this routine was done using the analytic solution that can be obtained in case of a homogeneous particle. First of all, it should be noted that the transmission probability and the escape probability can be derived analytically for a homogeneous sphere as detailed in the following subsections. These probabilities can be used to verify the collision probability since the volume-to-volume probabilities can be converted into to the volume-to-surface escape probabilities and then to transmission probability using the reciprocity relation between the escape probability and the first flight blackness and the balance condition for the transmission probability and the first flight blackness. In the following, a partial verification of the collision probabilities obtained from the SYBALS routine is performed by comparing with the analytic results of the transmission and escape probabilities.

2.4.1 Transmission Probability

Assume that a grain has K layers. External radius of layer k of grain i is given by r_{ik}^s . The total cross section of each layer is Σ_{ik} , and $r_{i0}^s = 0$. Considering the central symmetry of the problem, we can reduce the problem to the calculation of the transmission probability for the flat mono-directed source. Indeed, for the mono-directed uniform source the probability of entering at grain with the angle $\theta \in (\theta, \theta + d\theta)$ equals to:

$$p(\theta)d\theta = \frac{\cos \theta \cdot 2\pi R \sin \theta \cdot R d\theta}{\pi R^2} = 2 \cos \theta \sin \theta d\theta = 2\mu d\mu \quad (42)$$

where $2\pi R \sin \theta \cdot R d\theta$ gives the area of the strip shown in Figure 5. Distribution (42) is exactly the same angular distribution as for an isotropic source. Hence, the isotropic source can be replaced by a uniform mono-directed source for the sake of the transmission probability calculations.

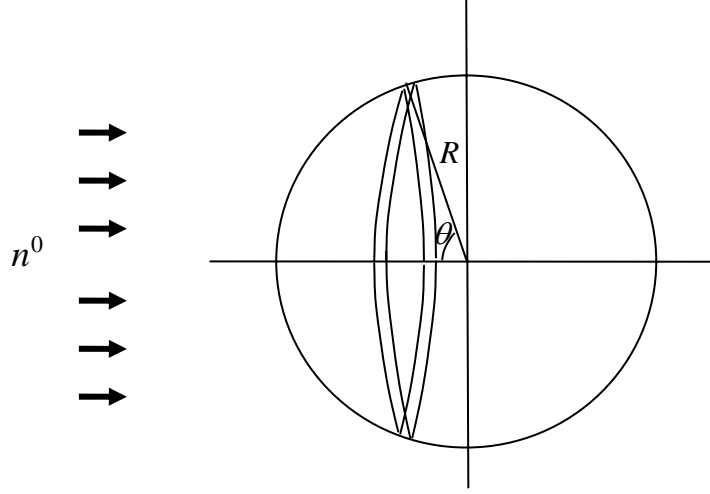


Figure 5. Evaluating of the angular probability density function for surface flux.

The transmission probability T_i^g is then obtained as in terms of the parameters defined in Figure 6:

$$T_i^g = \sum_{k=1}^K Z_k \quad (43)$$

$$Z_k = \frac{1}{\pi R^2} \int_{r_{k-1}}^{r_k} 2\pi r \cdot \text{Exp}\left[-\sum_{k=k'}^K g_{k'}(r)\right] dr \quad (44)$$

$$g_{k'}(r) \equiv \begin{cases} 2 \cdot \left(\sqrt{(r_{ik'}^g)^2 - r^2} - \sqrt{(r_{ik'-1}^g)^2 - r^2} \right) \cdot \Sigma_{ik'} & , \quad \text{for } k' > k \\ 2 \cdot \left(\sqrt{(r_{ik'}^g)^2 - r^2} \right) \cdot \Sigma_{ik'} & , \quad \text{for } k' = k \end{cases} \quad (45)$$

Integrals (44) can be evaluated numerically by using standard Gauss integration. In case of the homogeneous grain case, the integration (44) can be performed analytically resulting:

$$T = \int_0^R \frac{2r}{R^2} e^{-\Sigma \sqrt{R^2 - r^2}} dr = \frac{1 - e^{-2R\Sigma} - 2R\Sigma e^{-2R\Sigma}}{2R^2 \Sigma^2} \quad (46)$$

For the case of $\Sigma = 1/R$, the following results are obtained from the analytic expression and also from the SYBALS routine

Analytical solution : 0.29699708

SYBALS solution : 0.29699705.

This confirms that the SYBALS collision probability calculation is accurate.

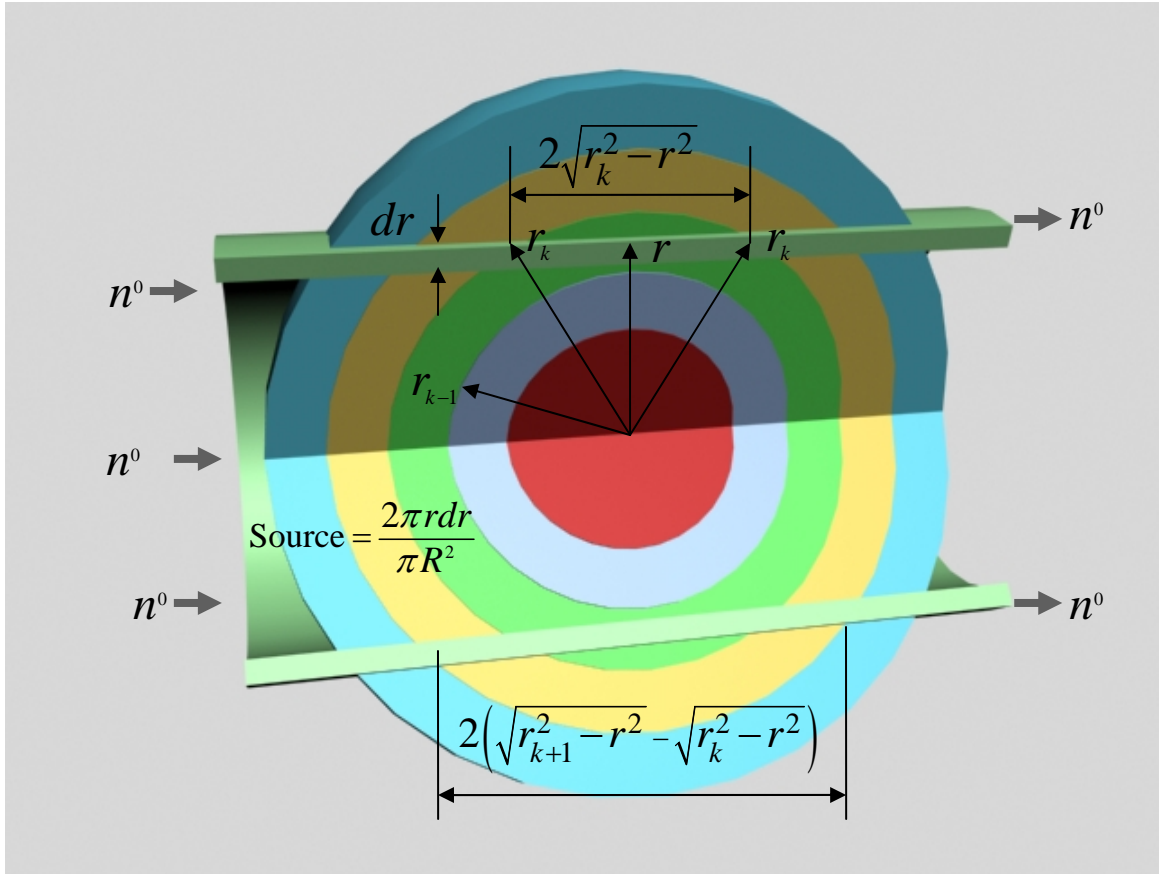


Figure 6. Configuration and parameters to calculate transmission probability

2.4.2 Volume-to-Surface Escape Probability

Assume that we have a sphere of radius R with uniformly distributed mono directed source of neutrons, emitting $3/4R^3$ neutrons per unit time and unit volume. Then, number of neutron per unit time emitted by disk $D = \{r \in [r, r + dr], h \in [h, h + dh], \phi \in [0, 2\pi]\}$ equals to:

$$S^* = \frac{3}{4\pi R^3} \cdot 2\pi r \cdot dr dh \quad (47)$$

while the quantity

$$\frac{3re^{-\Sigma h} dr dh}{2R^3} \quad (48)$$

gives the number of neutrons leaving from the sphere where h is the distance from the annular disk to the surface of sphere. Integration over range $h \in [0, 2\sqrt{R^2 - r^2}]$ gives the total amount of neutrons leaving from the cylinder:

$$D = \left\{ r \in [r, r + dr], h \in [0, 2\sqrt{R^2 - r^2}], \phi \in [0, 2\pi] \right\}$$

depicted in Figure 7. Finally, the integration over range $r \in [0, R]$ gives the number of neutrons leaving the sphere per unit time. Considering that total number of emitted neutrons per unit time equals to one, we can write the final expression for the escape probability as:

$$E = \frac{3}{4\pi R^3} \int_0^R dr \int_0^{2\sqrt{R^2 - r^2}} dh 2\pi r e^{-\Sigma h} = 3 \cdot \frac{2R^2 \Sigma^2 - 1 + (1 + 2R\Sigma)e^{-2R\Sigma}}{8R^3 \Sigma^3} \quad (49)$$

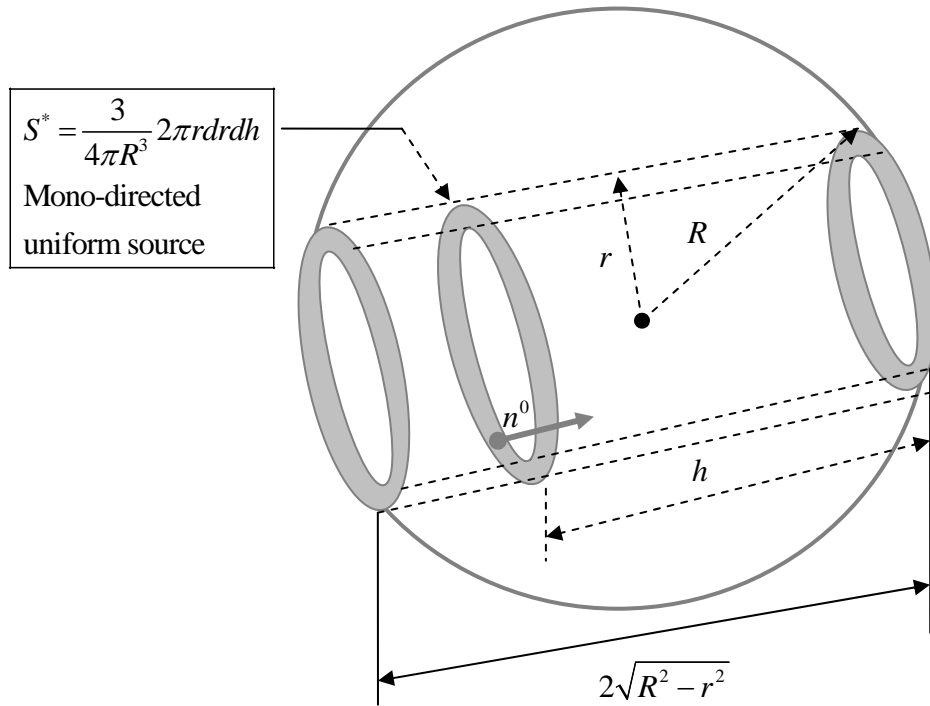


Figure 7. Configuration and parameters to calculate escape probability

For the case of homogeneous grain with $\Sigma = 1/R$, the following results are obtained for the escape probability:

Analytical solution : 0.527252194

SYBALS solution : 0.527252183

This is another indication that the SYBALS routine works fine.

3. Specifics of DH MOC Implementation into DeCART

For the implementation of the DH MOC, it is necessary to introduce another level of region which is for the microscopic regions inside triso grains. This region is named **subregion** since they belong to the already defined flat source region (FSR). In the subregion, the source and the material composition is regarded constant. The subregions are defined only for the composite material region which consists of the base matrix material and embedded grains. The material composition which specifies the each layer of the grain is also newly defined as the **micromaterial** in order to distinguish it from the noncomposite materials. If the fuel compact has N -kinds of grains each having 5 layers, there will be $5*N+1$ micromaterials to be defined. The number of subregions in this case is $5*N$ since the base region is reserved for the matrix. Since the flux and the source should be defined for each subregion, the region dependent variables should have another index to designate the subregion. The cross section variables need one more index to represent the micromaterial. The first step of modifying the DeCART routines was to change the structure of the relevant variables. The second step was then to implement the pre and post processing for the DH MOC calculation starting from the geometrical and material input for the micromaterials. The code modification and implementation of another level of loops to take care of the micromaterials are described below. The new input data and description are also given.

3.1 Change of Variable Structure

As the first step of modification, all the scalar variables defined for region such as the regionwise scalar flux, source and transport cross sections were replaced by vectors which have one additional micromaterial. Specifically, an additional array index was added to represent the micromaterial in the `xsreg(:,:)` array. The micromaterial index was added in arrays `siglp`, `sigps`, `phi`, `phiangsub` and others. There were also newly added variables to define composites. The full list of extended variables is given in Table 1. The variable structure change required a huge DeCART modification, but fortunately it was a formal operation that could be performed in a semi-automatic way. No additional cycle by micromaterials and no complicate logical changes were assumed at the first step. For the debugging purpose, only the first entry of the vectorized variables was be treated explicitly. Numerical results obtained after the first step change were the same as the ones from the original DeCART.

Table 1. List of Variables Newly Added or Modified

FORTRAN VARIABLE	MEANING
m	material ID in the key DH related subroutines. Index m spans homogeneous and heterogeneous material as well. It is exact number coming from material card at DeCART input (see DeCART manual)
mcmat	Index of micromaterial
mcmat1	Address of base material, usually =1
icomposite	Index of current composite material
itriso	Index of current type of triso particle
ilayers	Index of current layer in triso
ilayersd	Index of current layer in subdivided triso
matcomp(m)%n_constituting_mat	Number of constituting micro-materials in current homogeneous or composite material
matcomp(m)%mcmat_end	Length of cycle by micro-materials
matcomp(m)%mcmat_hom	Address of homogenized material (=7)
matcomp(m)%icomposite	Variable to save number of current micro-material
matcomp(m)%nref_mat(mcmat)	ID of homogeneous material, corresponding to micro material defined by mcmat
matcomp(m)%vol_frac_composite_mat(mcmat)	Volume fraction of current micro-material
composite%r(icomposite,itriso,ilayers)	External radius of current triso-layered
composite%rd(icomposite,itriso,ilayersd)	External radius of current subdivided triso-layered
composite%pf(icomposite,itriso)	Packing fraction
composite%pkd(icomposite,itriso,ilayersd)	volume fraction of subdivided layer respectively to composite material
composite%imaterial(icomposite)	ID of composite material (=m)
composite%matrix_mat(icomposite)	ID of base (matrix) material
composite%nrtriso(icomposite)	Number of types of triso particles
composite%nlayers(icomposite,itriso)	number of layers in current triso
composite%nlayersd(icomposite,itriso)	number of layers after subdivision
composite%ndiv(icomposite,itriso,ilayers)	user-specified subdivision of current layer
composite%mat(icomposite,itriso,ilayers)	
xsreg(ir,iz,mcmat1)%p0	volume fraction of matrix
xsreg(ir,iz,mcmat1)%lami(itriso)	Average chord of triso
xsreg(ir,iz,mcmat1)%sigik(ilayersd,itriso)	total XS of current layer
sigt_cp(ilayersd)	total XS in array for collision probability subroutine
r_cp(ilayersd)	radiuses for collision probability subroutine
xsreg(ir,iz,mcmat1)%sigaik(ilayersd,itriso)	absorption macro XS for MOC-DH preprocessor
xsreg(ir,iz,mcmat1)%sigsik(ilayersd,itriso)	scattering macro XS for MOC-DH preprocessor
xsreg(ir,iz,mcmat1)%egik(1:n_cp,itriso)	Escape probabilities by formula (14)
xsreg(ir,iz,mcmat1)%sig_tilda	sigma tilda, by formula (8)
xsreg(ir,iz,mcmat1)%e_hat_gik(1:nlayersd,itriso)	E-hat, by formulae (16)
dh_correction(ifs)	Renormalization factor by form. (10)

3.2 Program Logic Changes

The second step of changes consists of 1) updating the input processor to define properties of composite materials (number of micromaterials in current composite material, cross sections of micromaterials, geometry of triso particles and packing fraction); 2) updating everywhere in DeCART the branched logic of elemental region treatment, depending on internal micro-structure (homogeneous or not), 3) updating cycle by micromaterials in every part of DeCART dealing with the treatment of composite region, 4) updating the pre and post processor of ray tracing (modification in the SUBGFSP.F subroutine), 5) extension of the flux convergence acceleration technique for the case of composite materials (unlike to conventional case, we need accelerate the flux convergence of several fluxes per each region, namely flux in matrix and flux in each layer of triso-particle).

Thus, from the point of view of programming, the following four basic modifications was done:

- 1) updating of new micro heterogeneity driving index in all variables, related with transport equations (cross sections, neutron fluxes, regionwise reaction rates),
- 2) updating logic of handling of two different kinds of regions (homogeneous and micro-heterogeneous),
- 3) updating cycle by the micro-heterogeneity driving index
- 4) updating Sanchez-Pomraning pre and post processor for ray tracing subroutine to calculate neutron fluxes inside carbon matrix and at all layers of all kinds of triso particles.

3.2.1 Two Loops to Treat Micromaterials

There was two additional loops to incorporate the micromaterials. The first loop type is required for pre and post processing ray tracing procedure when we explicitly need to handle each triso particle, say for calculation collision probabilities. The second loop type is used when we simply need to process all micro materials regardless of its belonging to the triso particles or the base matrix material. Such type of cycle arises during scattering of fission source calculations.

Consider a loop of the first type. The following code segment consisting of 3 nested cycles t shows in term of standard DeCART-DH variables how to perform nested cycle by triso

particles, triso layers and triso sublayers. Here the outermost loop, with header “do itriso=1,ntriso” is the cycle by kinds of triso particles. The loops with header “do ilayers=1,nlayers” spans all layers of current triso particle. Finally the loop with header “do idiv=1,ndiv” spans sublayers of the triso particle.

```

!   initiate micromaterial index
!   (usually mcmat=1 for matrix, 2 for fuel kernal etc )
mcmat=1
!   assign ID number of current material
m=celtyp(ictp)%ireg(irl)
!   assign logical variable, which is .true.
!   for composite material and .false. for homogeneous
lcomposite=matcomp(m)%lcomposite
!   exit from subroutine, if material is homogenous
if(.not.lcomposite) return
!   assign ID number of composite material
icomposite=matcomp(m)%icomposite
!   assign number of kinds of triso particles
!   at current composite material
ntriso=composite%ntriso(icomposite)
!   cycle by triso particles
do itriso=1,ntriso
!   assign number of layers in current triso particle
nlayers=composite%nlayers(icomposite,itriso)
!   initiate counter of layers in current triso-particle
ilayersd=0
!   cycle by layers
do ilayers=1,nlayers
!   assign theuser-specified subdivision of layer.
ndiv=composite%ndiv(icomposite,itriso,ilayers)
!   cycle by subdivision
do idiv=1,ndiv
!       Naming convention: d - points in
!                               subdivision-related
!                               variables
!       update index of layer
ilayersd=ilayersd+1
!       .....
!       update micro-material index
mcmat=mcmat+1
enddo ! end of sublayers (idiv)
enddo ! end of layers (ilayers)
!   remembering total number of subdivided layers
nlayersd=ilayersd
enddo ! end of triso (itriso)

```

Consider now the loop of second type. The code segment of the *setrtfsp* subroutine given below shows how to treat the micromaterials in a region. The loop is incorporated by the new micro material index *mcmat*. Loop by *mcmat* was incorporated inside the ordinary DeCART loop. The end of loop is defined by the *mcmat_end* parameter. A typical value of *mcmat_end* can be 1 for a homogeneous material and 6 for the simplest composite material consisting of only one type of grain having 5 layers. In case of a composite material,

$mcmat=1$ corresponds to the base matrix material, $mcmat=2$ corresponds to the triso kernel, $mcmat=3$ corresponds to the second triso layer end so on. In case of two or more triso particles, the counting of $mcmat$ starts from the matrix material, then it continues from the kernel of the first triso particle up to external layer, then it continues from the kernel of the second type triso particle and so on. So it is accumulated. Usually address $mcmat_end+1$ is reserved for smeared composite material.

```

do l=myxyb,myxye
  ic=lc2m(l)
  ictp=icels3d(iz,cell2d(ic)%itype)
  iregfst=cell2d(ic)%iregfst
  ia=lctoa(l)
  do ii=1,celtyp(ictp)%nxsreg
    ir=cell2d(ic)%ixsregfst+ii-1
!   determine inscattering element in p0 scat matrix
    mcmat_end=xsreg(ir,iz,mcmat1)%mcmat_end
    do mcmat=1,mcmat_end
      call xseclgp0(xsreg(ir,iz,mcmat)%niso,
+          xsreg(ir,iz,mcmat)%temp,
+          xsreg(ir,iz,mcmat)%idiso,
+          xsreg(ir,iz,mcmat)%pnum,jgrp)
!     Setup scattering source tsrc
      do j=jssrcfr(jgrp),jssrcto(jgrp) ! Scat j->jgrp
        do ifsl=1,celtyp(ictp)%nregxsreg(ii)
          ifs=iregfst+celtyp(ictp)%mapxs2reg(ifsl,ii)-1
!         here tsrc is source for fixed source problem
          tsrc(ifs,mcmat)= tsrc(ifs,mcmat)+
+            xsmacs(j,jgrp)*phisdh(ifs,iz,j)%mat(mcmat)
        enddo ! of ifsl
      enddo ! of j
    enddo ! of mcmat
  enddo ! of ii
enddo

```

The essential benefit of using cycle of the second type comes from the possibility of unified treatment of heterogeneous and homogeneous regions. The only difference between the homogeneous and heterogeneous materials lies in the loop bound - $mcmat_end$.

3.2.2 Non-Iterating Part of Ray Tracing Preprocessor

This part of the preprocessor calculates all variables that can be determined only once before flux iterations. It was realized in subroutine *repdh* which calculates the following paramters:

$p_{ik}, \tilde{\Sigma}, \Sigma, r_c, P_{ik;il}^g, V_{il}^g, E_{ik}^g, \hat{E}_{ik}^g$. These values are calculated for each region designated by standard DeCART indices ir, iz , then are stored in the *xsreg* structure with address $mcmat1$, corresponding to the base matrix material. For example, variable `xsreg(ir,iz,mcmat1)%sig`

contains the homogenized cross section, calculated for the MOC region designated by radial index ir and axial index iz . Variable `xsreg(ir,iz,mcmat1)%e_hat_gik(1:nlayersd,itriso)` contains reduced escape probabilities \hat{E}_{ik}^g for the region designated by ir, iz , for triso particle $itriso$. The preprocessor is bypassed, if material is homogeneous.

3.2.3 Modification of Ray Tracing Driver Routines

The MOC calculation is performed for two purposes in DeCART. The first one is to solve the subgroup fixed source problem and the other is to actually solve the transport problem. The MOC calculation for the subgroup calculation is driven by `subgrfsp` and the other one is by `moc`. The following modifications were introduced to `subgrfsp`.

- 1) updating loop by micro-material,
- 2) setting up sources for subgroup fixed source problem
- 3) invoking of non-iterated part of ray tracing preprocessor.
- 4) updating iterating part of ray tracing preprocessor
- 5) ray trace post-processing to obtain fluxes in subregions

The iterating part of the preprocessor calculates values $q_{ik}, q_0, \Phi_{as}, q$. These values are defined by formulae (17)-(20). The postprocessor calculates values $\bar{\Phi}_0, \Phi_{ik}, \bar{\Phi}_{ik}$, defined by formulae (22)-(24).

The modifications of the MOC subroutine is similar to those described above except for the calculation of sources q_{ik}, q_0 in which the fission and scattering source must be incorporated.

3.3 Input Description and Sample Inputs

DeCART-DH has the same input as the usual DeCART except for the DH related blocks and cards which is listed below.

Table 2. Micro Material Input Description

Card	Format	Variable	Description
Block: COMPOSITE_MATERIAL			
1	I	%imaterial	Composite material numeric ID
1	I	%matrix_mat	Material of matrix
1	I	%i_homo	Homogenization option 0 – DH, 1-Homogenization
Block: TRISO_PARTICLE			
1	I	%nlayers	Number of layers
1	R	%pf	Volume fraction for this particle
2	R	%r	External radiuses of layers
3	I	%mat	Constituent material of triso-layers
4	I	%ndiv	Number of subdivisions of each layers

Block COMPOSITE_MATERIAL includes only one card to assign two variables: composite%imaterial(icomposite), composite%matrix_mat(icomposite) where icomposite is a index of the composite material incrementing inside input subroutine. Composite material numeric ID plays the same role as Mixture numeric ID in the conventional DeCART. Both of IDs can be used in GEOM block of DeCART to refer the material in the conventional way, regardless whether the material is homogeneous or not.

Block TRISO_PARTICLE should follows block COMPOSITE_MATERIAL. It can be repeated several times which means that a composite material includes several kinds of triso particles. The first card defines two variables composite%nlayers(icomposite,itriso) and composite%Pf(icomposite,itriso) - the number of layers and the volumetric fraction of current triso particle, respectively. Here, *icomposite* is a the counter of the composite material. The second card defines variable composite%r(icomposite,itriso,1:nlayers) where itriso is the counter of triso particles for the current composite material. The expression 1:nlayers defines the length of input vector. The external radii of the triso-layers should be in one string in the increasing order. The third card defines vector composite%mat(icomposite,itriso,1:nlayers). Material IDs should be listed in one string, in the order from the centre to periphery. The fourth card defines composite%ndiv(icomposite,itriso,1:nlayers) variable which specifies the number of subdivision triso-layers in the DH MOC calculation. The recommended value is one, that means no subdivision.

A sample of input is given below. It is quoted from a *k-eff* benchmark calculation for a typical VHTGR fuel cell for the problem specification given in Section 4 .

```

MATERIAL
  mixture    1 UO2  2 10.41 27.0 / 92235 2.34176e-3 92238 2.10758e-2 8016 4.68352e-
2
  mixture    2 C    1 1.05 27.0 / 6000 0.0526455
  mixture    3 C    1 1.9  27.0 / 6000 0.0952632
  mixture    4 SiC  1 3.18 27.0 / 6000 0.0477608 14000 0.0477608
  mixture    5 CMA  1 1.2  27.0 / 6000 0.0601663
  mixture    6 CBL  1 1.74 27.0 / 6000 0.0872411
  mixture    7 Hom  2 1.65 27.0 / 92235 6.61369e-5 92238 5.95232e-4 8016 1.32274e-
3 6000 0.0613356 14000 2.83716e-3
  mixture    8 GAP  1 0.01 27.0 / 6000 0.05e-7
  mixture    9 Hom  2 1.65 27.0 / 92235 6.61369e-5 92238 5.95232e-4 8016 1.32274e-
3 6000 0.0613356 14000 2.83716e-3
COMPOSITE_MATERIAL  9 5 0 ! assigned number of "mixture", material of matrix
TRISO_PARTICLE     6 0.28916 ! number of layers, volume of this particle
0.0175 0.0275 0.0310 0.03455 0.0380 3.80001e-2
1      2      3      4      3      7
1      1      1      1      1      1
COMPOSITE_MATERIAL 10 5 0 ! assigned number of "mixture", material of
matrix
TRISO_PARTICLE     6 0.14458 ! number of layers, volume of this particle
0.0175 0.0275 0.0310 0.03455 0.0380 3.80001e-2
1      2      3      4      3      7
1      1      1      1      1      1
TRISO_PARTICLE     5 0.14458 ! number of layers, volume of this particle
0.0175 0.0275 0.0310 0.03455 0.0380
1      2      3      4      3
1      1      1      1      1.

```

4. Verifications of the Implementation

In order to verify the implementation of the DH MOC solution into DeCART, several tests have been made during various stages of the implementation. The first type of the verification was to verify the collision probability and consequent escape probability calculated by SYBALS as explained in Section 2.3. The final test was for the actual doubly heterogeneous problem for which a Monte Carlo reference solution is available. The intermediate verifications include the verification of the subregion flux compared with the collision probability based solution, the comparison of the solution of the subgroup fixed source problem for the zero-leakage case with the analytic solution, the comparison of the resonance cross section between the heterogeneous and homogeneous particles, and some other testes listed in Table 3. In the following, some of the intermediate verifications and the final verification is described.

Table 3. Verification of stochastic effective cross section

N	Test	Purpose	Result
1	Explicit DH treatment for an artificial problem where the matrix and triso particles are composed of the identical material to obtain <i>effective stochastic</i> cross section which can be compared to the analytic solution.	To verify all terms of nonlinear equation for <i>effective stochastic</i> cross section (9). To verify convergence of non-linear iterations (9) to a true value of <i>effective stochastic</i> , regardless of the choice of initial guess.	Obtained a full agreement between numerical and analytical solution
2	Calculation of <i>effective stochastic</i> cross section for heterogeneous case to make sure that resulting cross section obeys theoretical bounds given in Reference 오류! 책갈피가 정의되어 있지 않습니다..	To justify <i>effective stochastic</i> cross section in heterogeneous case.	Effective cross section belongs to the analytically estimated range given at Physor2004 Sanchez paper.

4.1 DH MOC Subgroup Solution for a Single Cell

In DeCART, the resonance scattering is not explicitly considered so that the resonance fixed source problems of Eq. (2) becomes simply:

$$\hat{\Omega} \cdot \nabla \varphi_m(\vec{r}, \hat{\Omega}) + (\Sigma_{am}(\vec{r}) + \Sigma_p(\vec{r})) \varphi_m(\vec{r}, \hat{\Omega}) = \frac{1}{4\pi} \lambda \Sigma_p(\vec{r}) + \frac{1}{4\pi} (1 - \lambda) \Sigma_p(\vec{r}) \int_{4\pi} \varphi_m(\vec{r}, \hat{\Omega}) d\hat{\Omega} \quad (50)$$

For a homogeneous cell with the reflective condition leading to zero leakage which can be constructed by assigning identical materials to all the constituents of the fuel cell (matrix material=triso material), three terms of neutron transport equation can be cancelled as shown in equation (51).

$$\begin{aligned} & \cancel{\hat{\Omega} \cdot \nabla \varphi_m(\vec{r}, \hat{\Omega})} + (\Sigma_{am}(\vec{r}) + \cancel{\Sigma_p(\vec{r})}) \varphi_m(\vec{r}, \hat{\Omega}) = \\ & = \frac{1}{4\pi} \lambda \Sigma_p(\vec{r}) + \frac{1}{4\pi} (\cancel{\Sigma_p(\vec{r})} - \lambda \Sigma_p(\vec{r})) \int_{4\pi} \varphi_m(\vec{r}, \hat{\Omega}) d\hat{\Omega} \end{aligned} \quad (51)$$

due to that $\varphi_m(\vec{r}, \hat{\Omega}) = \frac{1}{4\pi} \int_{4\pi} \varphi_m(\vec{r}, \hat{\Omega}) d\hat{\Omega}$ at our specific test problem. Then the analytical solution is:

$$\varphi_m(\vec{r}, \hat{\Omega}) = \frac{1}{4\pi} \frac{\lambda \Sigma_p(\vec{r})}{\Sigma_{am}(\vec{r}) + \lambda \Sigma_p(\vec{r})} \quad (52)$$

$$\Phi_m(\vec{r}) = \int_{4\pi} d\hat{\Omega} \varphi_m(\vec{r}, \hat{\Omega}) = \frac{4\pi}{4\pi} \frac{\lambda \Sigma_p(\vec{r})}{\Sigma_{am}(\vec{r}) + \lambda \Sigma_p(\vec{r})} = \frac{\lambda \Sigma_p}{\Sigma_{am} + \lambda \Sigma_p} \quad (53)$$

It was verified that the solution of DeCART DH subgroup FSP gives the same solution as the analytic ones.

The resonance cross sections obtained for the heterogeneous case and the homogeneous case are now compared in Table 4 which reveals a significant decrease in the heterogeneous case due to the enhanced self-shielding.

4.2 Micro Heterogeneity Only

Suppose a fuel cell containing only the fuel compact, i.e. carbon matrix with triso particles. With the reflective boundary condition, the infinite medium of the heterogeneous random mixture shown in can be modeled with the DeCART DH MOC flux solver. A reference solution for this problem can be obtained independently by solving the neutron transport equation for single triso-particle, surrounded by carbon matrix with reflective boundary condition at the external boundary. The configuration is shown in Figure 8. The external radius is obtained as:

$$R_{triso+carbon} = \frac{R_{triso}}{\sqrt[3]{V_f}} \quad (54)$$

Table 4. Effective random media cross section (Σ_{tot}) in the resonance range.

Group N	Hetero ^{*)}	Homo ^{**)}	Difference in shielded XS (%)
10	0.0009614	0.0009644	0.3100502
11	0.0027077	0.0027642	2.0439910
12	0.0064637	0.0067314	3.9768845
13	0.0064708	0.0067037	3.4742008
14	0.0114180	0.0119660	4.5796423
15	0.0114060	0.0119210	4.3201074
16	0.0088502	0.0089166	0.7446785
17	0.0079102	0.0079553	0.5669177
18	0.0024774	0.0024774	0.0000000
19	0.1053000	0.1133000	7.0609003
20	0.0183820	0.0184600	0.4225352
21	0.0025503	0.0025499	-0.0156869
22	0.0036905	0.0036987	0.2216995
23	0.0009813	0.0009808	-0.0499597
24	0.0025314	0.0025332	0.0710564
25	0.0021887	0.0021891	0.0182723
Σ (10-25)	0.1942896	0.2041117	4.8121212

*) Double heterogeneous UO₂ shielding, then volume weighted XS homogenization.

***) Triso-particles and carbon matrix homogenized prior performing DeCART calculations.

where V_f is volumetric fractions of triso-particles in fuel compact to preserve the volumetric fraction of triso-particle in the matrix. The solution of this problem can be obtained semi-analytically by employing the collision probability formula:

$$\Phi_i = \sum_{j=1}^n \tilde{P}_{ij} q_j \quad (55)$$

where $q_j = (\lambda \Sigma_p)_j$. The collision probability kernel \tilde{P}_{ij} can be obtained from the collision probabilities P_{ij} by imposing the reflective boundary condition. The SYBALS routine gives both P_{ij} and \tilde{P}_{ij} .

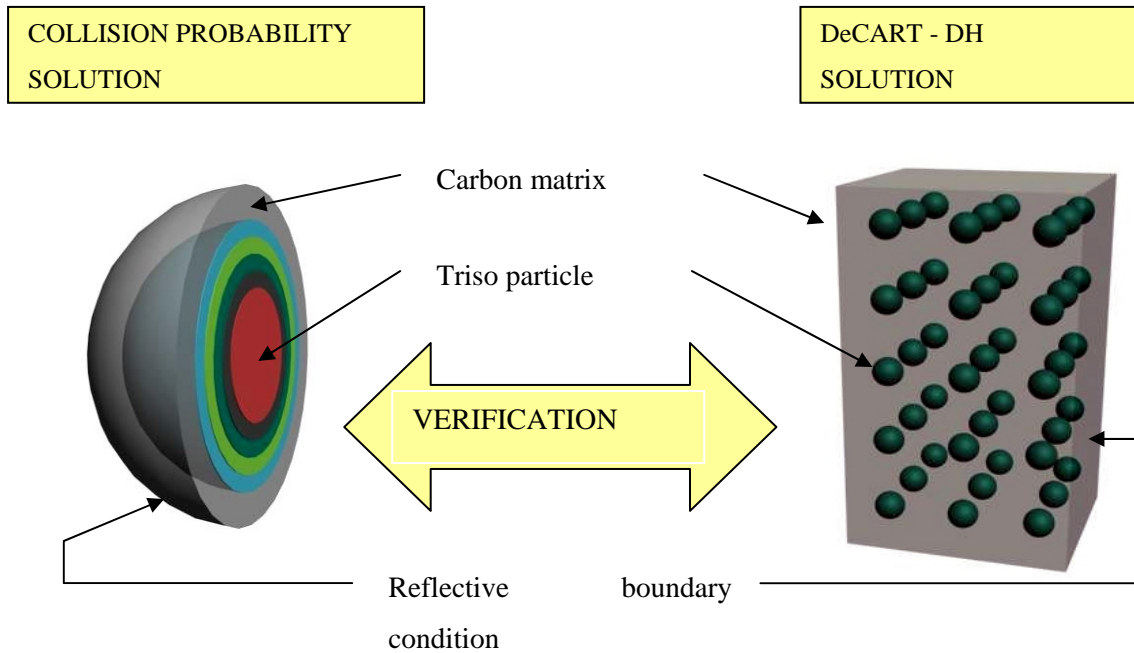


Figure 8. Infinite medium of composite material to be represented by a single triso model

The result of this comparison is given in Table 5 in terms of the flux distribution within the triso. The data were obtained from the subgroup fixed source problem for resonance group 1, category 1, subgroup level number 4 (the biggest one for U238). It can be proved by this table that the accuracy of DeCART-DH in the really heterogeneous test is quite good.

Table 5. Flux distribution inside triso-particle obtained by DH MOC and CP

Layer	MOC DH solution	CP Solution
1	0.13132	0.13145
2	0.22443	0.22490
3	0.24040	0.24121
4	0.24375	0.24488
5	0.24569	0.24735
6	0.25118	0.24959

4.3 Macro-heterogeneity Only at the Pin Cell Level

The DH MOC solver can also solve the singly heterogeneous problem in which no triso particles are included. This proves the modification to realize the double heterogeneity has been done properly. In order to confirm this, a single pin-cell was solved by the original DeCART and DeCART-DH. The DeCART DH solution was generated for the fuel compact, where the material properties of each layer of the triso particles were set to identical to the

volume-weighted material property of the fuel compact. Therefore the DH algorithm was employed to processing the pin cell with homogenized fuel compact. As the result, a full identity was obtained between the DeCART DH and DeCART solutions.

4.4 Assessment of DH effect in Practical Problems

The final verification of the DH treatment capability of the DeCART-DH was performed by assessing the DH effect for a fuel pin cell and for a pin-gas hole checkerboard problem. The MCNP solutions for the exactly same problems were taken as the reference. In the MCNP calculations, the micro heterogeneity was explicitly represented. The DH effect is calculated as the difference in the reactivity of the heterogeneous and homogeneous cases. In order to the temperature dependency of the DH effect, 3 fuel temperatures were examined. The specification of the triso and compact and the triso packing fraction (29.7%) was obtained from the NGNP design. The hexagonal fuel cell was converted to a square cell. The 190 group cross sections were used in the DeCART calculation while the continuous energy cross sections generated from ENDF-B/VI Rel.8 was used in the MCNP calculations. The problem specification for the heterogeneous case is shown in Table 6 while the smeared number densities are given in Table 7. The geometry of the single pin cell and the checkerboard problem is shown in Figure 9.

The DeCART-DH calculation was performed twice. The first case is to consider the DH effect only in the subgroup FSP which gives the shielded resonance cross section with the DH effect. In this case, the normal MOC transport calculation was done without the DH MOC solver. The second case is for the full DH effect consideration which invokes the DH-MOC calculation in the normal transport calculation. In the first case, the DH effect is partially covered since the DH effect due to the high cross section at the thermal range is not considered. As shown in Table 8, which summarizes all the results, the DH effect ranging from 2400 to 4300 pcm is well predicted by the DeCART DH solver with the largest error of about 280 pcm as long as the full DH treatment is performed. It is worthwhile to note that the DH effect solely due to the resonance cross section is only 55~67% so the DH treatment in the normal MOC transport calculation is very important as well.

Table 6. Specification of fuel cell with explicit micro heterogeneity

Composition		Material	Radius (cm)	Nuclide	Density (g/cm ³)	Atomic Number density
Triso Particle	Fuel Kernel	UCO	0.0175	U-235	10.5	2.1146E-2
				U-238		2.4754E-3
				O-16		3.5432E-2
				C		1.1811E-2
	Buffer	Carbon	0.0275	C	1.00	5.0192E-2
	Inner Pyro-Carbon	Carbon	0.0310	C	1.90	9.3858E-2
	Silicon Carbide	SiC	0.0345	Si	3.20	4.8081E-2
C				4.8081E-2		
Outer Pyro-Carbon	Carbon	0.0385	C	1.87	9.3858E-2	
Compact matrix		Carbon	0.6225	C	1.1995	6.0205E-2
Coolant		He	0.6350	He	0.0032	4.7744586E-4
Graphite block		Carbon		C	1.74	8.7311663E-2

Table 7. Specification of fuel cell with smeared micro heterogeneity

Composition	Material	Radius (cm)	Nuclide	Density (g/cm ³)	Atomic Number density
Fuel	UCO Carbon SiC	0.6225	U-235		6.9025876E-5
			U-238		5.8965063E-4
			C		6.1717100E-2
			O-16		9.8801197E-4
			Si		2.8200119E-3
Coolant	He	0.6350	He	0.0032	4.7744586E-4
Graphite block	Carbon		C	1.74	8.7311663E-2

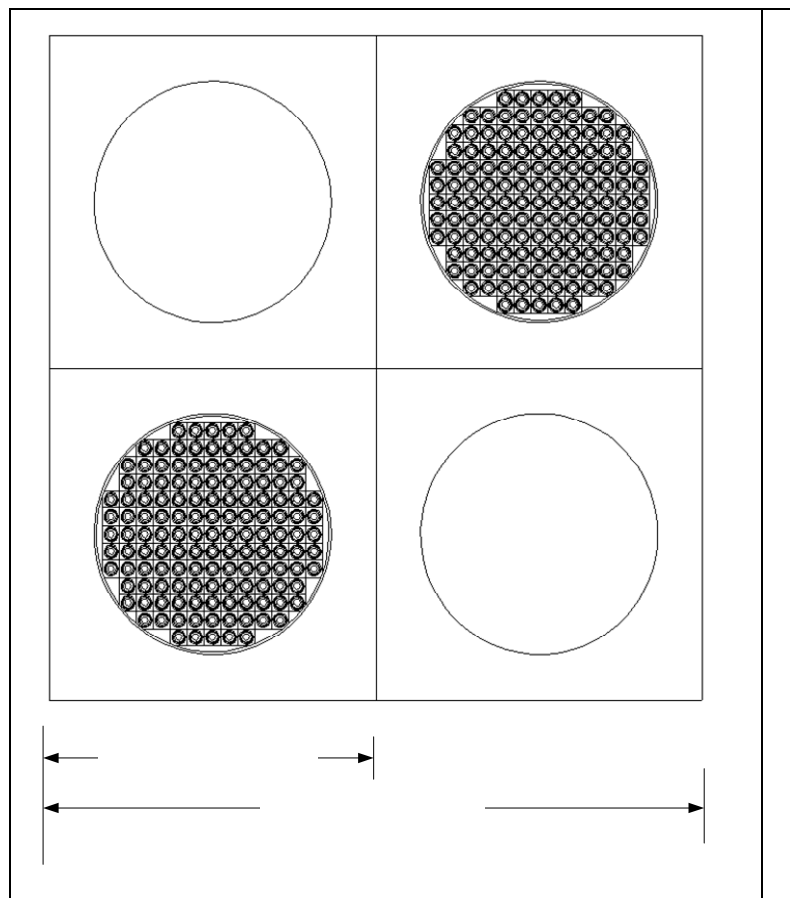
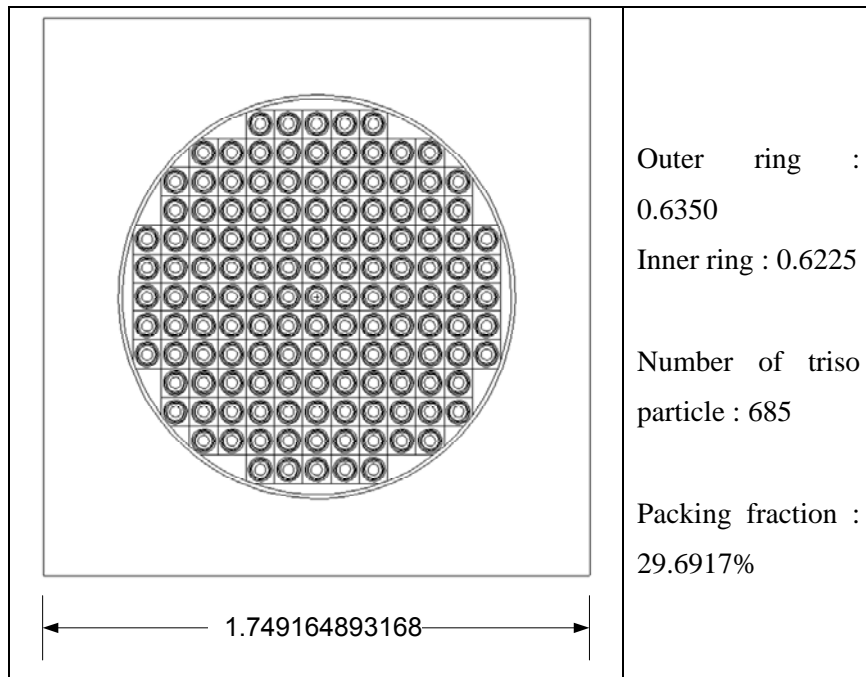


Figure 9. Configuration of the single pin cell and the checkerboard problema

Table 8. DH Effect at various conditions and calculation options

Structure	Temperature	Program	Material	k-inf	Δk	MCNP-DeCART ¹⁾
1x1	300k	MCNP	DH	1.41680	3318	66.7%*
			Homogenized	1.35318		
		DeCART Reso. Only	DH	1.40114	2024	1294
			Homogenized	1.36250		
		DeCART Full	DH	1.42114	3035	283
			Homogenized	1.36238		
	600k	MCNP	DH	1.36309	3900	59.5%
			Homogenized	1.29429		
		DeCART Reso. Only	DH	1.34130	2160	1740
			Homogenized	1.30354		
		DeCART Full	DH	1.36811	3631	269
			Homogenized	1.30337		
900k	MCNP	DH	1.32418	4310	54.5%	
		Homogenized	1.25269			
	DeCART Reso. Only	DH	1.29721	2207	2102	
		Homogenized	1.26110			
	DeCART Full	DH	1.32871	4049	261	
		Homogenized	1.26088			
2x2	300k	MCNP	DH	1.56594	2362	68.2%
			Homogenized	1.51008		
		DeCART Reso. Only	DH	1.55126	1514	848
			Homogenized	1.51566		
		DeCART Full	DH	1.56820	2220	143
			Homogenized	1.51545		
	600k	MCNP	DH	1.52264	2734	60.5%
			Homogenized	1.46179		
		DeCART Reso. Only	DH	1.50274	1585	1149
			Homogenized	1.46779		
		DeCART Full	DH	1.52618	2621	113
			Homogenized	1.46748		
	900k	MCNP	DH	1.49015	2952	55.2%
			Homogenized	1.42736		
		DeCART Reso. Only	DH	1.46625	1592	1360
			Homogenized	1.43281		
		DeCART Full	DH	1.49413	2883	69
			Homogenized	1.43243		

^{1),*} The values given in % is the fraction of the DH effect on the resonance cross section only to the whole DH effect.

5. Conclusions

The Sanchez-Pomraning method to resolve the double heterogeneity effect in the MOC transport calculation was successfully implemented into the DeCART code. Although the implementation required a significant amount of changes in the coding in order to handle the micromaterials and subregions properly, the primary changes themselves were straightforward involving pre and post processing prior to the standard MOC calculation. The preprocessing is needed to determine the effective stochastic cross section of the composite and also to set the effective source. The preprocessing step requires the calculation of the escape probabilities for the triso particle which was made possible using a collision probability routine for a heterogeneous sphere. No significant modification of the MOC routine was required since the characteristics of the MOC problem for the doubly heterogeneous medium is identical except that the outgoing current of each region is to be augmented by the renormalization factor. The postprocessing after the MOC calculation which is to determine the flux and reaction rates in the subregions is also very quite straightforward. The DH implementation was done for both the subgroup fixed source problem and the normal transport problem.

The verification of the DH MOC solver was done in several ways including the comparison with analytical solutions obtainable in simplified cases. All the verification showed satisfactory results. Particularly, the final verification involving the pin cell and checkerboard calculations with and without the DH representation confirmed that the DH effect of about 3000 pcm can be predicted well with the DeCART DH solver with the maximum error of 280 pcm. It is quite noticeable that the DH treatment is needed not only for the resonance cross section generation but also for the normal transport calculation since the DH effect on the resonance cross section results in only about 60% of the total DH effect.

Currently, the CMFD acceleration has not been implemented for the DH solver. It can be done without much effort by extrapolating the subregion flux as well. The implementation of the CMFD acceleration should be done in parallel with the extension of the DH solver to the hexagonal geometry.

References

1. H. G. JOO, J. Y. CHO, K. S. KIM, C. C. LEE, and S. Q. ZEE, "Methods and Performance of a Three-Dimensional Whole-Core Transport Code DeCART," *Proc. PHYSOR2004*, CD-ROM, Chicago, Illinois, USA, April 25-29, 2004.
2. R. Sanchez and G.C. Pomraning, "A statistical analysis of the double heterogeneity problem," *Ann. Nucl. Energy*, **18**, 371 (1991).
3. R. Sanchez and E. Masiello, "Treatment of the double heterogeneity with the method of characteristics," *Proc. PHYSOR2002*, Seoul, Korea, 2002.
4. Han Gyu Joo and Tong Kyu Park, "Derivation of Analytic Solution and MOC Calculation Procedure for Double Heterogeneity Treatment," SNURPL-SR-001(07), Department of Nuclear Engineering, Seoul National University (2007)
5. A Kavenoky, Calcul et utilisation des probabilités de première collision pour des milieux hétérogènes à une dimension: Les programmes ALCOLL et CORTINA, Note CEA-N-1077, Commissariat à l'énergie atomique, Saclay, France (1969).
6. G. Marleau, DRAGON THEORY MANUAL, PART 1: COLLISION PROBABILITY CALCULATIONS, Report IGE-236, Institut de génie nucléaire, École Polytechnique de Montréal, Montréal, Québec (1999).